PNAS
www.pnas.org

Supplementary Information for

Active dendrites enable strong but sparse inputs to determine orientation selectivity

Lea Goetz, Arnd Roth & Michael Häusser

Michael Häusser
Email: m.hausser@ucl.ac.uk

This PDF file includes:

Supplementary text
SI Reference
Figures S1 to S9
Table S1
Legend for Movie S1

Other supplementary materials for this manuscript include the following:

Movie S1

Supplementary Information Text

Detectors of dendritic Na^+ spikes, NMDA spikes and bAPs

Na^+ spikes

To distinguish dendritic Na^+ spikes from fast EPSPs, we compared a fully active model and a model in which dendritic Na_v conductances were switched off (1) (see Figure 2) in a subset of simulations. We defined an increase in local dendritic event amplitude of >10% from passive to active, i.e. the difference between the active and passive dendritic voltage as a fraction of the baseline-subtracted passive voltage, as the threshold of an active event. Since this typically corresponded to a dendritic g_{Na} of more than 0.3 mS/cm^2 (*SI Appendix*, Fig. S4*C*), we subsequently used this conductance density threshold as an efficient operational definition for the Na^+ spike detectors in our simulations (see Fig. 2*A*).

NMDA spikes

We detected NMDA spikes with both an NMDA current criterion and a local dendritic voltage criterion. The voltage criterion is equivalent to the local dendritic voltage exceeding a threshold of –40 mV for at least 26 ms (compare τ_{NMDA} = 26 ms). To meet the current criterion, synaptic current has to exceed 30% of the peak current through the NMDA conductance at –40 mV (≡ start of NMDA spike), and deliver inward charge greater or equal to 0.1 nA * ms, before returning to less than 15% of the peak current (≡ end of NMDA spike). The corresponding thresholds are 2.76 nA/μS * w and 1.38 nA/μS * w for the plateau start and plateau end current, respectively, where w is the synaptic weight. If the current criterion is met in a given segment, the voltage criterion has to be met in segments up to 50 μm from this segment for a transient to be classified as a NMDA spike. The function of this NMDA spike detector was verified by comparing the membrane potential trajectories in a fully active simulation and a simulation where the voltage dependence of NMDA conductances was frozen at its value at the resting potential (1) (see Fig. 2*B*).

Backpropagating APs (bAPs)

In experimental measurements, dendritic events that result from the backpropagation of somatic APs are difficult to distinguish from locally generated dendritic events because it is technically difficult to monitor both dendritic and somatic membrane potentials at the

same time. In the model, we detected an AP at the soma, using a voltage threshold of –30 mV, and followed its backpropagation in time into the dendritic arbor, providing a spatiotemporal bAP profile (latency and halfwidth) specific to each dendrite. If the detection of a candidate Na^+ spike fell into the spatiotemporal bAP profile for that dendrite – given the detection of a recent somatic AP initiation – the dendritic event was classified as a bAP, rather than a local Na^+ spike.

Occasionally, backpropagation slows down as the bAP reaches distances far away from the soma, resulting in latencies and amplitudes of local Na_v channel activations that differ from the characteristic bAP profile for a dendrite. Thus, as a further safeguard against misclassifying bAPs as locally generated events, we introduced a maximum (100) on the number of segments in which g_{Na} crosses threshold during a single dendritic Na^+ spike. Combined with the profile matching procedure, this robustly discriminated between dendritic events resulting from backpropagation of APs and locally generated dendritic events.

SI Reference

1. M. Rapp, The computational role of excitable dendrites. (PhD thesis, Hebrew University, Jerusalem, Israel, 1997).

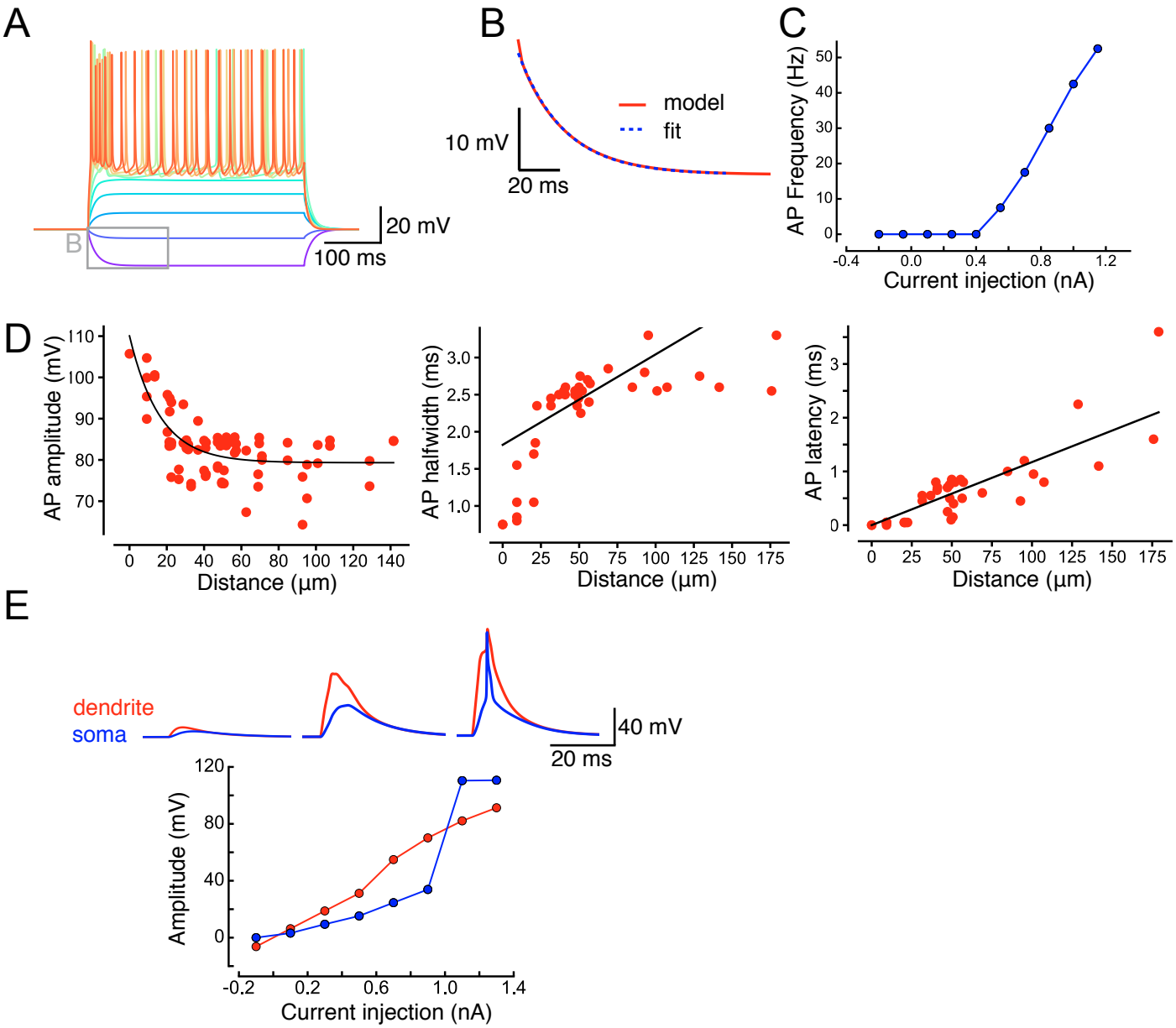

Fig. S1. Validation of the postsynaptic neuron model.

(A) Model responses to somatic current injection. (B) Exponential fit of membrane time constant (blue, dashed) to a response to negative current injection (inset in A) (C) Frequency-current relation obtained from current injections shown in A. (D) Left, decrement in the amplitude of backpropagating APs with distance from the soma. Black line shows an exponential fit, $\lambda = 46\ \mu m$. Center, half-width of backpropagating APs increased with distance from the soma. Black line, linear fit. Right, latency of backpropagating APs. Propagation velocity (linear fit, black line) was $v = 179\ \mu m/ms$. (E) Response to dendritic current injection, measured at the dendritic location of injection (red) and at the soma (blue). Example traces at the top show responses to subthreshold (left), dendritic suprathreshold (center) and somatic suprathreshold (right) current injections. Note how the dendritic nonlinearity is more shallow than the somatic nonlinearity.

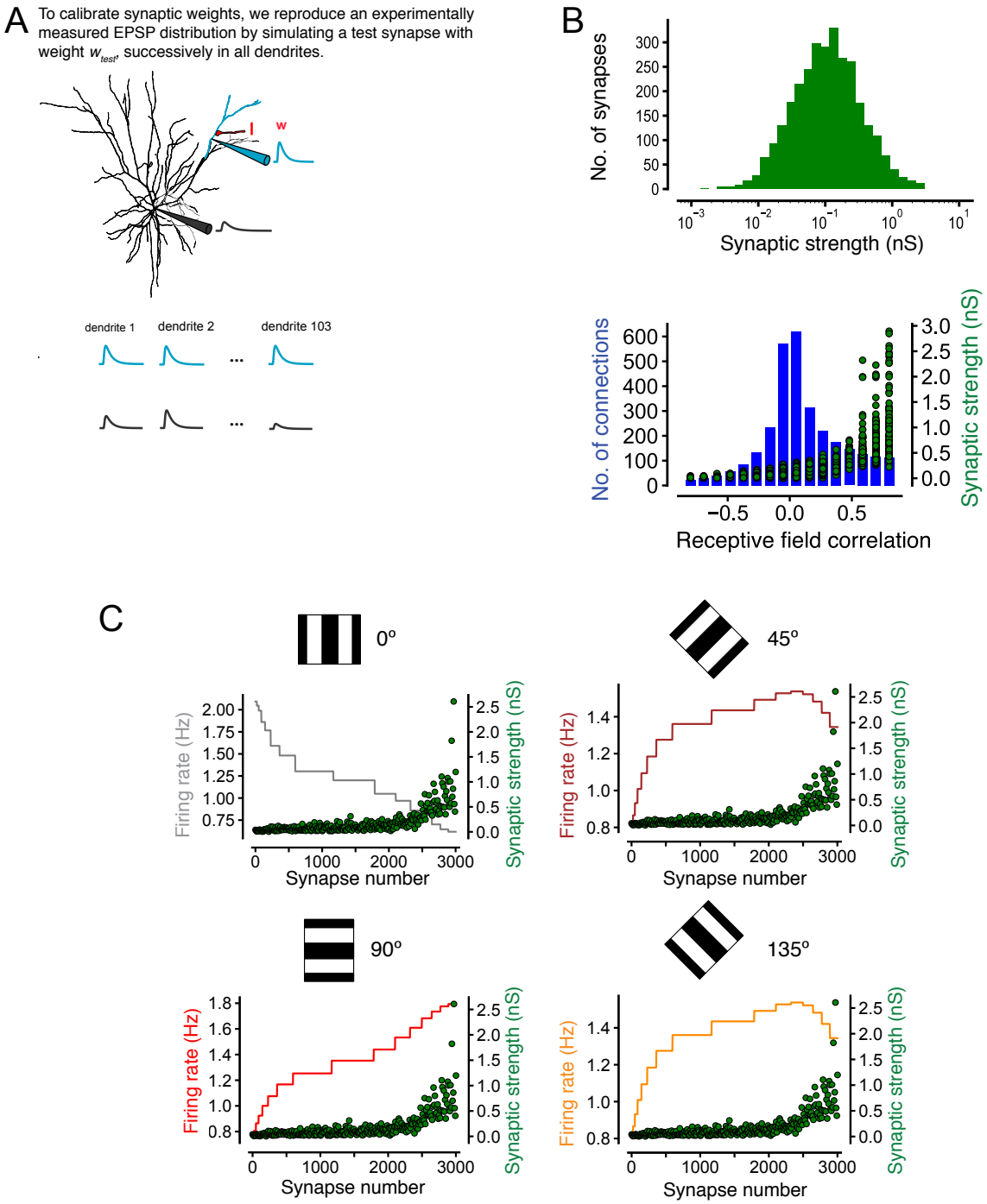

Fig. S2. Validation of the presynaptic input model, including calibration of synaptic weights.

(A) Protocol for determining the parameters of the lognormal distribution of synaptic input weights. Briefly, to translate the measured somatic EPSP amplitude into a peak conductance of a synaptic contact, we measured the average effect at the soma of a 1 nS synapse placed on each dendrite in turn. We scaled this by the number of synaptic contacts per single-axon connection and adjusted it to fit the measured somatic EPSP distribution (Cossell et al., 2015). (B) Top, the resulting lognormal distribution of all synaptic input weights. Bottom, blue bars, number of connections (i.e., synaptic inputs to the postsynaptic neuron) in 16 bins of receptive field correlation of the presynaptic input and the postsynaptic neuron (see Cossell et al., 2015). Bottom, green dots, synaptic strengths of inputs in different presynaptic-postsynaptic receptive field correlation bins. (C) Definition of 0°, 45°, 90° and 135° stimulus orientations. Cityscape histograms, presynaptic firing rate as a function of synapse number. Green dots, a representative subset of synaptic strengths in B as a function of synapse number. The postsynaptic neuron is by definition tuned to the 90° orientation, thus for the 90° orientation, strong synaptic inputs receive high firing rates (the high-frequency tail of a normal distribution of firing rates), whereas for the 0° orientation, weak synaptic inputs receive high firing rates. The orientations 45° and 135° lie in-between.

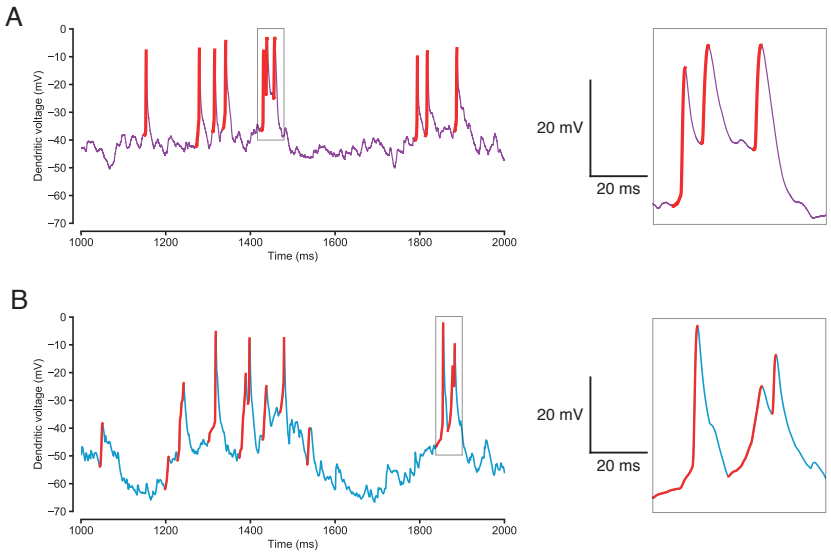

Fig. S3. Detection of dendritic events using a threshold on dV/dt and a minimum voltage amplitude criterion.

(A) Representative recording of dendritic voltage (purple) from L2/3 pyramidal neuron in vivo from Smith et al. (2013), with detected events (red). Inset: magnification of grey rectangle. (B) Representative recording of dendritic voltage (light blue) in biophysical model, with detected events (red). Inset: magnification of grey rectangle. Events are stretches of monotonically increasing membrane potential with an amplitude threshold of 10 mV.

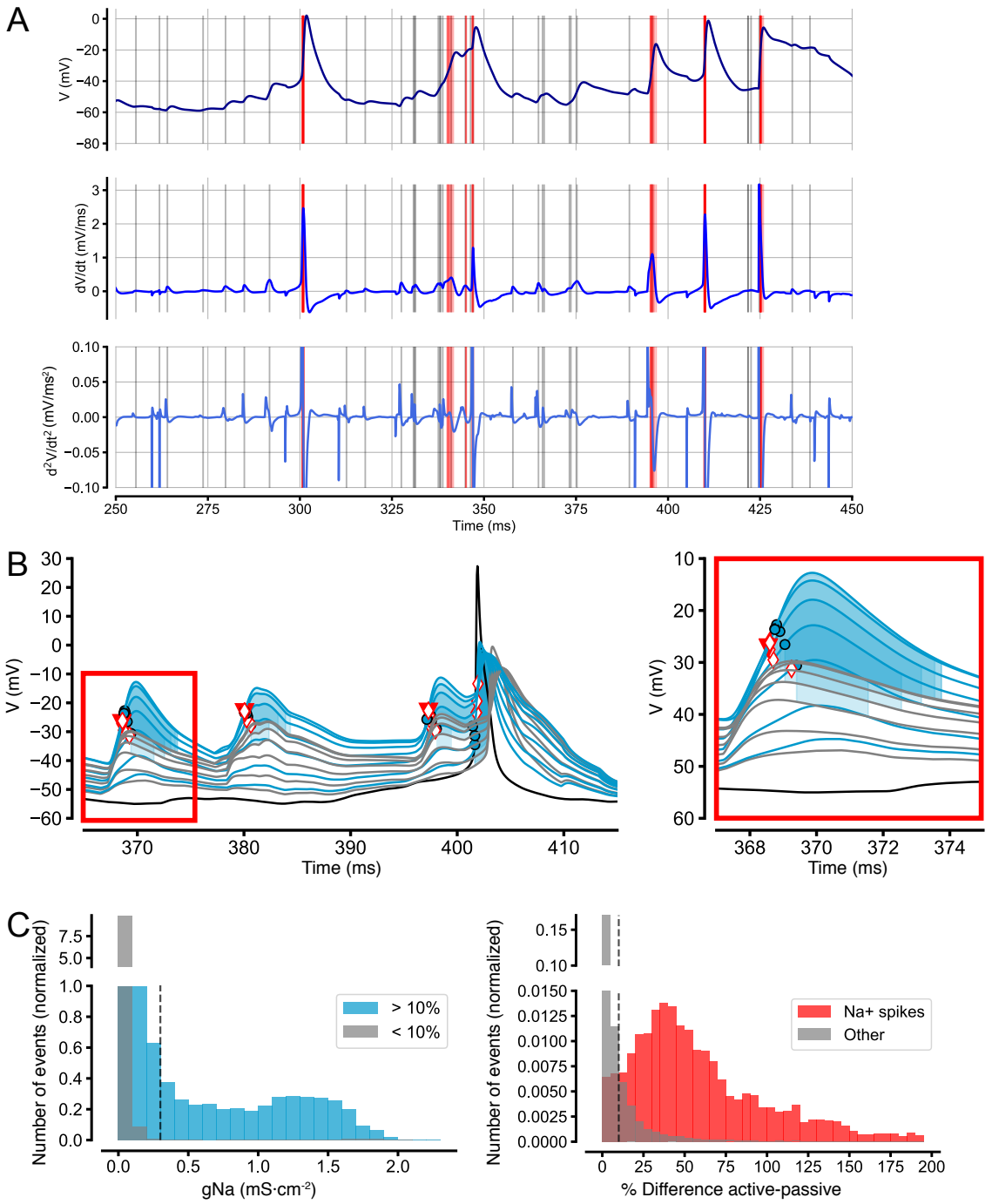

Fig. S4. Definition of dendritic Na^+ spikes.

(A) Comparison of dendritic Na^+ spikes as detected by a local dendritic Na^+ conductance criterion (red vertical lines, each line represents the detection in one segment of the recorded dendrite; see Methods for a description of the g_{Na} criterion) and a theoretical criterion of an inflection point in the second derivative of the local dendritic voltage and event amplitude ≥ 10 mV (vertical grey lines, each line represents detection in one segment of the recorded dendrite). (B) Comparison of initiations of dendritic Na^+ spikes as detected by a local dendritic Na^+ conductance criterion (red triangles: Na^+ spike initiation; white diamonds: Na^+ spike propagation) and a 10% active-passive difference criterion (blue dots and blue shading; the semi-transparency allows the identification of the overlap in shadings between different segments) between the local dendritic voltage in all segments of an example dendrite during an active (light blue) and a passive (grey) simulation. Somatic voltage shown in black. Inset: magnification of a dendritic Na^+ spike shown on left (red rectangle). (C) Left: distribution of events across all dendrites with an active-passive difference greater than (blue) or smaller than (grey) 10% of the passive dendritic voltage. The false positive rate (the percentage of events with less than 10% active-passive difference that are above the g_{Na} threshold) is 0.4%. Right: distribution of active-passive differences of the passive dendritic voltage for events detected as dendritic Na^+ spikes (red) or EPSPs (grey). The false negative rate (the percentage of events below the g_{Na} threshold that have more than 10% active-passive difference) is 7.95%.

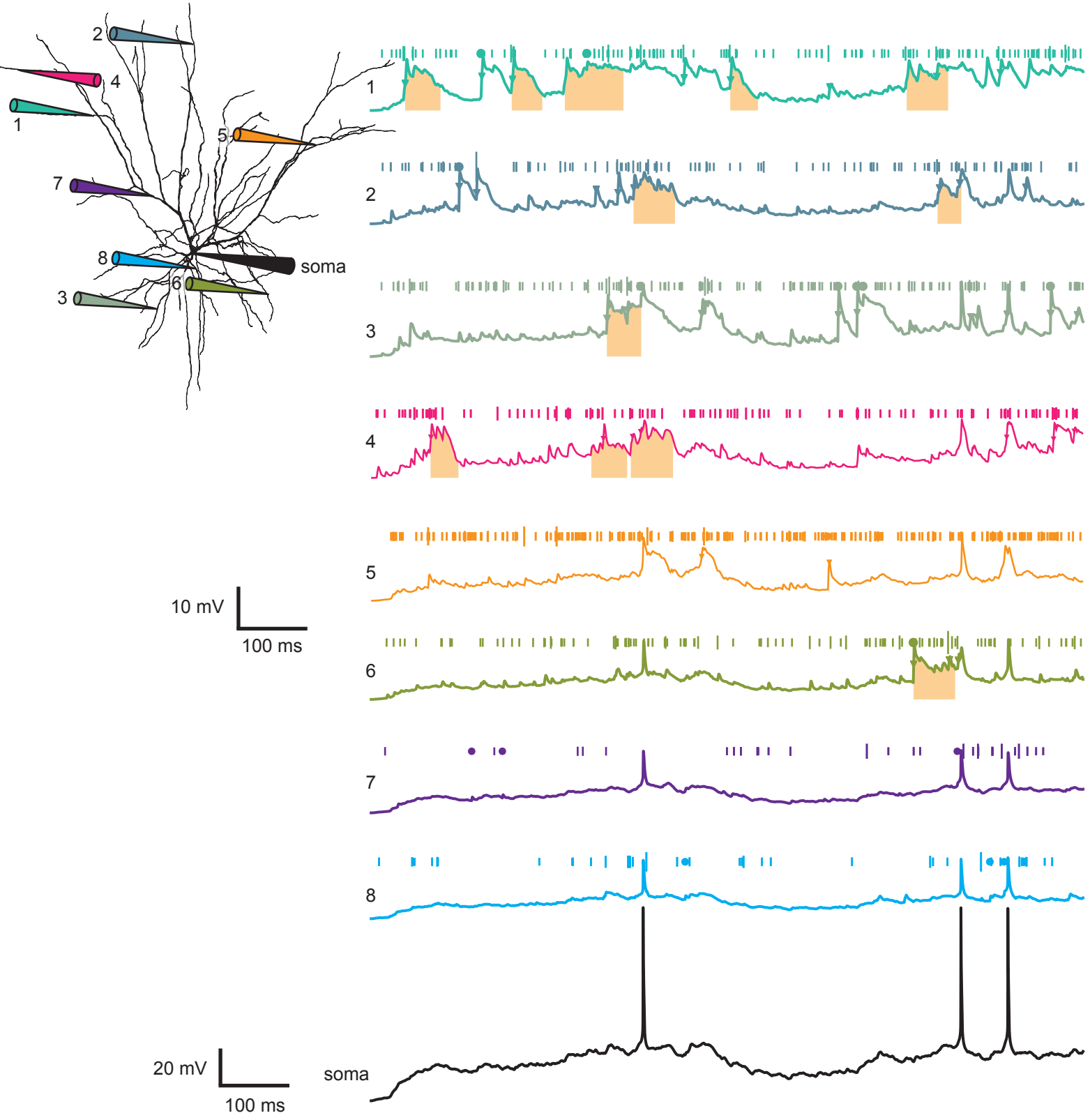

Fig. S5. Visualization of location and time courses of dendritic Na^+ spikes and NMDA spikes on the neural morphology.

Morphology of the neuron (left) with indications of recording locations for 8 dendritic membrane potential traces (right). Recordings are made at the location of the strongest synapse on that dendrite. The spike-times of this strongest synapse are indicated with a dot, along with the spike times of all other synapses on that dendrite (indicated with a vertical bar, scaled by synaptic weight). The bottom trace shows the membrane potential at the soma, allowing back-propagating APs to be clearly identified in all dendritic traces. Dendritic Na^+ spikes are indicated with inverted triangles, dendritic NMDA spikes are shaded in orange.

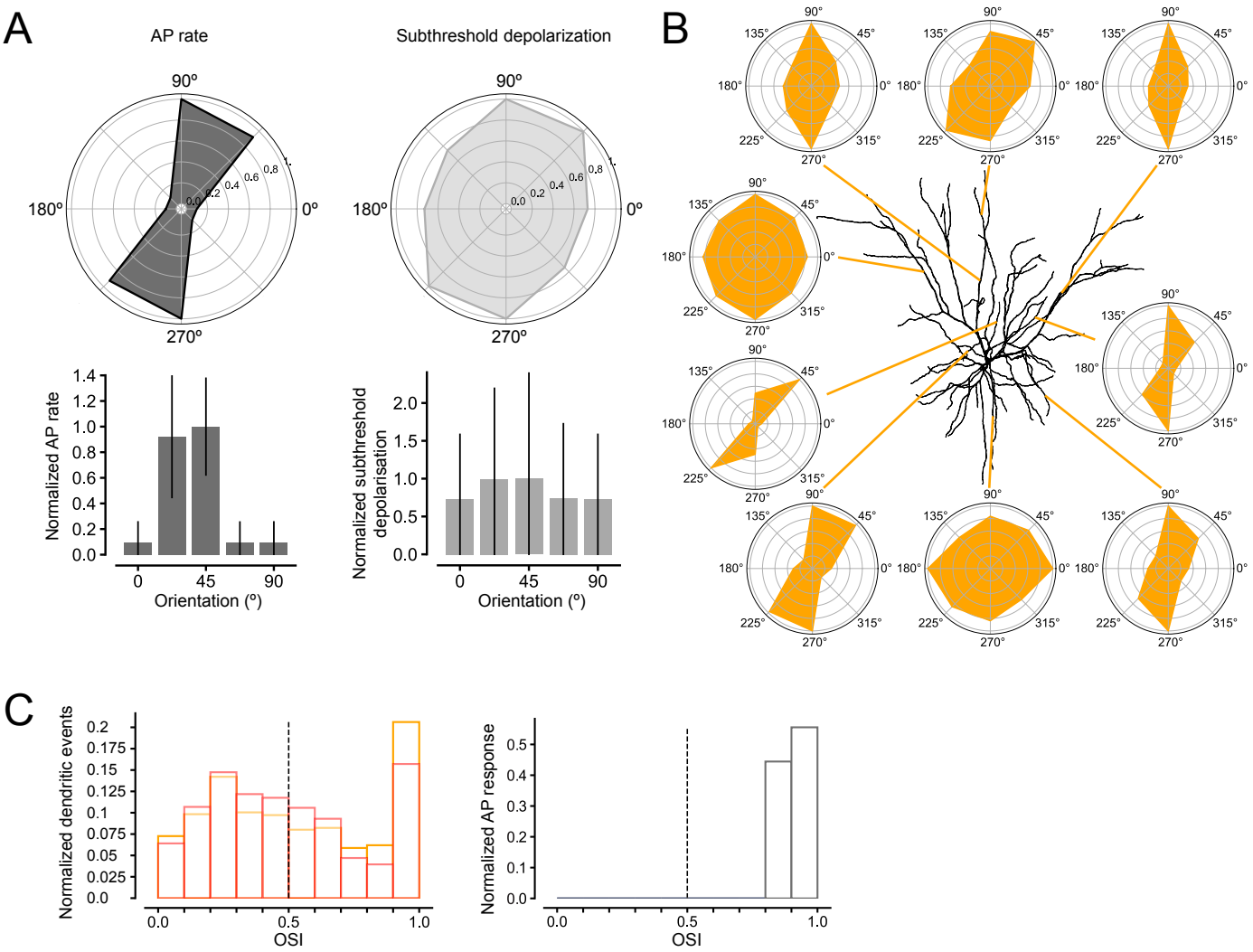

Fig. S6. Reproducing experimental results from Jia et al. (2010).

(A) Top: Example tuning for somatic APs (dark grey) and somatic subthreshold membrane potential tuning (light grey). Bottom: average across different random seeds. Compare to Jia et al. (2010), Figure 1e-f. (B) Examples of heterogeneity and distribution pattern of orientation-tuned NMDA spikes on different dendritic branches. Compare to Jia et al. (2010), Figure 3c. (C) Input-output relationship in a highly tuned neuron. Orientation selectivity indices (OSIs) for dendritic events (left; red: dendritic Na^+ spikes; orange: dendritic NMDA spikes) and somatic AP output (right; dark grey). Compare to Jia et al. (2010), Figure 4d.

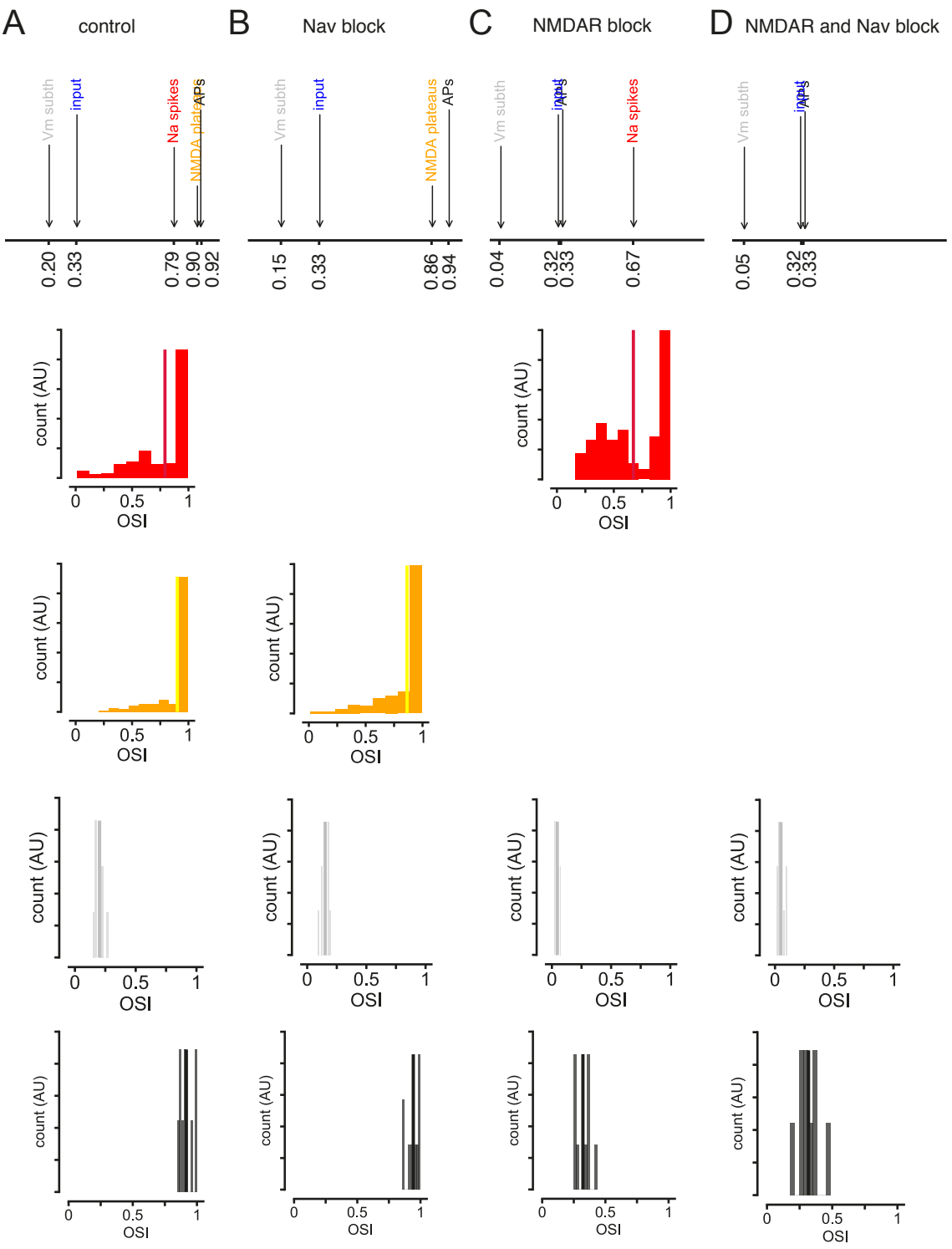

Fig. S7. Orientation Selectivity Index (OSI) under blockage of dendritic nonlinearities.

(A) Progression of mean OSI in the control condition (top), distribution of dendritic Na^+ spike OSI (second from top), distribution of NMDA spike OSI (third from top), distribution of somatic V_mOSI (fourth from top) and distribution of AP OSI (bottom). (B) Progression of mean OSI with dendritic Nav conductances blocked (top): corresponding distribution of dendritic Na^+ spike OSI (second from top), distribution of NMDA spike OSI (third from top), distribution of somatic V_mOSI (fourth from top) and distribution of AP OSI (bottom). (C) Progression of mean OSI when NMDAR conductances are frozen at the resting potential (top): corresponding distribution of dendritic Na^+ spike OSI (second from top), distribution of NMDA spike OSI (third from top), distribution of somatic V_mOSI (fourth from top) and distribution of AP OSI (bottom). (D) Progression of mean OSI when both dendritic Nav conductances are blocked and NMDAR conductances are frozen at the resting potential (top): corresponding distribution of dendritic Na^+ spike OSI (second from top), distribution of NMDA spike OSI (third from top), distribution of somatic V_mOSI (fourth from top) and distribution of AP OSI (bottom).

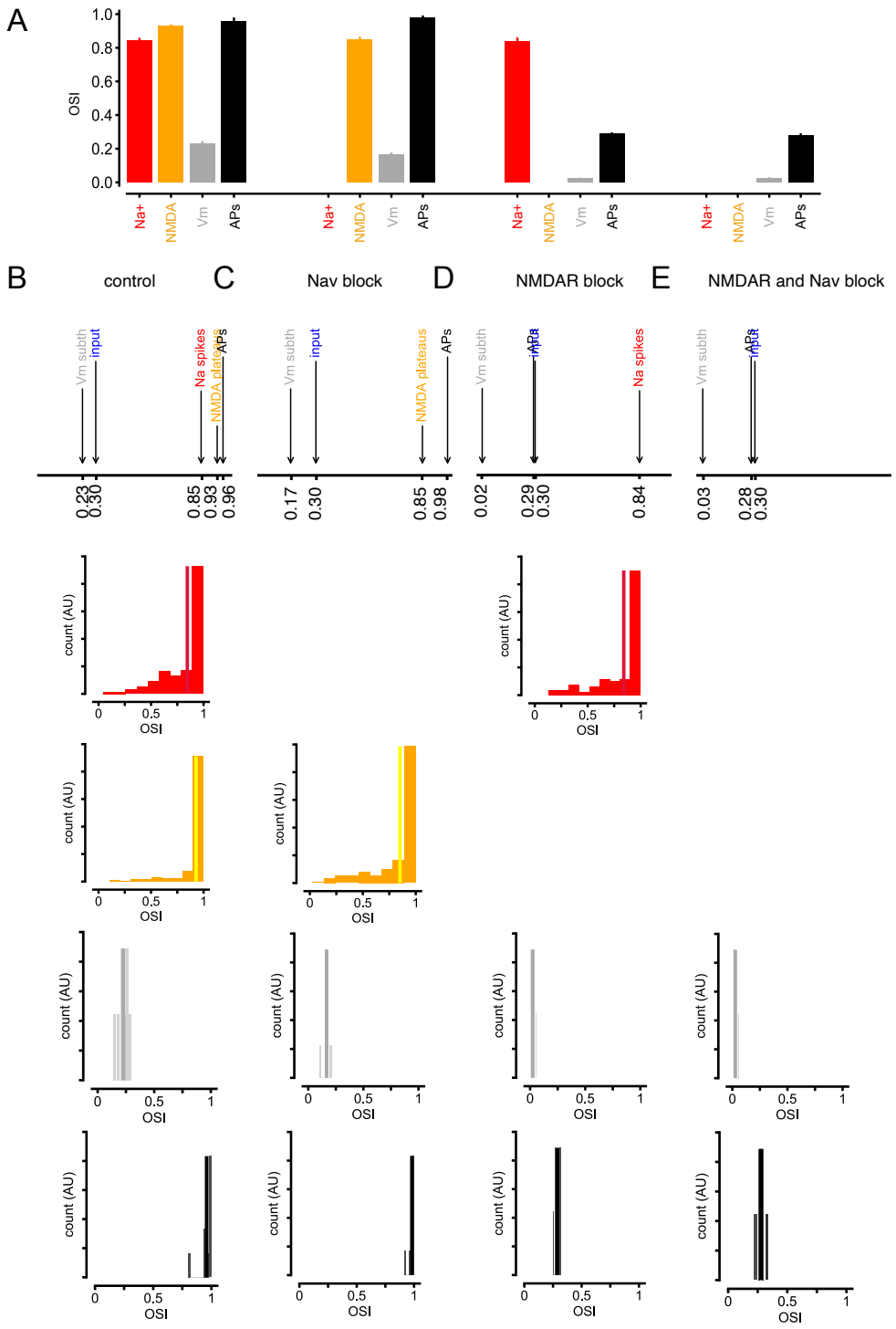

Fig. S8. Orientation Selectivity Index (OSI) under blockage of dendritic nonlinearities during clustered synaptic input.

(A) During clustered synaptic input, example of the tuning of dendritic Na^+ spikes (red) and NMDA spikes (orange) as well as subthreshold somatic membrane potential (grey) and APs (black), under control conditions and with dendritic Na^+ spikes (second from left), NMDA spikes (third from left) or both (right) blocked. (B) Progression of mean OSI in the control condition (top), distribution of dendritic Na^+ spike OSI (second from top), distribution of NMDA spike OSI (third from top), distribution of somatic V_mOSI (fourth from top) and distribution of AP OSI (bottom). (C) Progression of mean OSI with dendritic Nav conductances blocked (top): corresponding distribution of dendritic Na^+ spike OSI (second from top), distribution of NMDA spike OSI (third from top), distribution of somatic V_mOSI (fourth from top) and distribution of AP OSI (bottom). (D) Progression of mean OSI when NMDAR conductances are frozen at the resting potential (top): corresponding distribution of dendritic Na^+ spike OSI (second from top), distribution of NMDA spike OSI (third from top), distribution of somatic V_mOSI (fourth from top) and distribution of AP OSI (bottom). (E) Progression of mean OSI when both dendritic Nav conductances are blocked and NMDAR conductances are frozen at the resting potential (top): corresponding distribution of dendritic Na^+ spike OSI (second from top), distribution of NMDA spike OSI (third from top), distribution of somatic V_mOSI (fourth from top) and distribution of AP OSI (bottom).

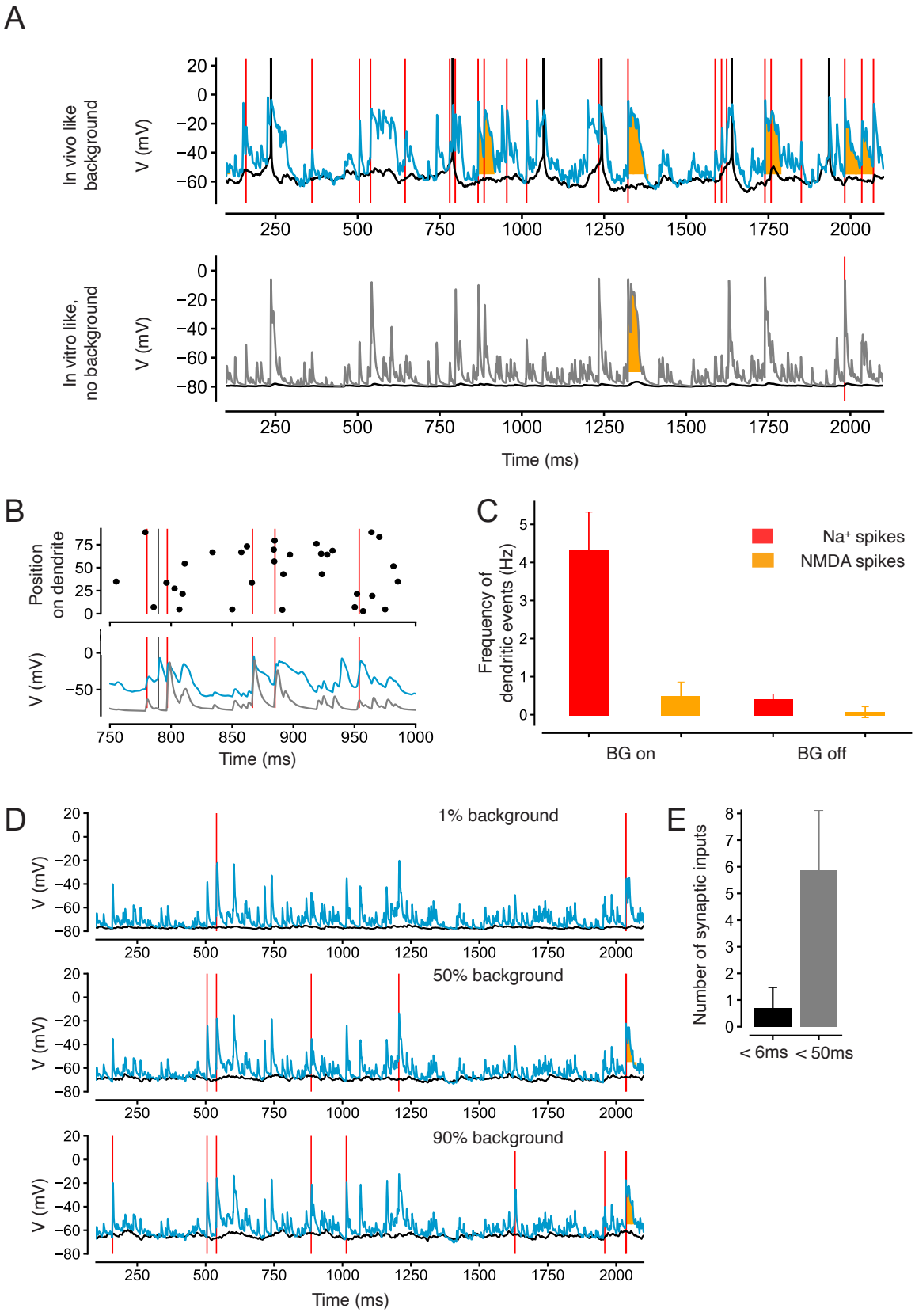

Fig. S9. Effects of varying background activity.

(A) Effect of abolishing background synaptic input on dendritic voltage (with background: top, light blue; without background: bottom, grey), somatic voltage (black) and initiation of dendritic Na^+ spikes (red vertical lines), NMDA spikes (orange shading) and bAPs (black vertical lines). (B) Direct comparison between dendritic voltage in full simulation (light blue) and simulation without background (grey), with dendritic Na^+ spikes (red vertical lines) and bAPs (black vertical lines). For reference, we show the synaptic inputs on the recorded dendrite (black dots). (C) Frequency of dendritic Na^+ spikes (red) and NMDA spikes (orange) in simulations with and without background activity. (D) Comparison of example dendritic voltage under reduced (1%, 50%, 90%) background activity, colors as for A. (E) Number of synaptic inputs falling within the summation window common in in vitro experiments (< 6 ms) and our detection windows (< 50 ms).

Table S1. Parameters describing the passive and active properties of the postsynaptic neuron model, related to Methods.

Soma:

Parameter	Value	Reference
E_K	-80 mV	Smith et al., 2013 (17)
E_{Na}	60 mV	"
E_{Ca}	140 mV	"
gNa_{soma}	80 mS*cm^{-2}	Schmidt-Hieber & Bischofberger, 2010 (103)
giA_{soma}	45 mS*cm^{-2}	Korngreen & Sakmann, 2000 (104)
gKslow	450 mS*cm^{-2}	"
gKm	0.22 mS*cm^{-2}	Smith et al., 2013 (17)
gKca	20 mS*cm^{-2}	"
gCa	0.1 mS*cm^{-2}	"
gCaT	0.3 mS*cm^{-2}	"

Axon, axon hillock and initial segment:

Parameter	Value	Reference
E_K	-80 mV	Smith et al., 2013 (17)
E_{Na}	60 mV	"
E_{Ca}	140 mV	"
gNa	30 mS*cm^{-2}	Schmidt-Hieber & Bischofberger, 2010 (103)
gNa_{hill}	180 mS*cm^{-2}	"
gNa_{iseg}	30 mS*cm^{-2}	"
giA	15 mS*cm^{-2}	Korngreen & Sakmann, 2000 (104)
giA_{hill}	36 mS*cm^{-2}	"
giA_{iseg}	15 mS*cm^{-2}	"
gKslow	60 mS*cm^{-2}	"
$gKslow_{hill}$	180 mS*cm^{-2}	"
$gKslow_{iseg}$	60 mS*cm^{-2}	"

Dendrites:

Parameter	Value	Reference
E_K	-80 mV	Smith et al., 2013 (17)
E_{Na}	60 mV	"
E_{Ca}	140 mV	"
gNa	5 mS*cm^{-2}	Schmidt-Hieber & Bischofberger, 2010 (103)
giA	2 mS*cm^{-2}	Korngreen & Sakmann, 2000 (104)
gKslow	1 mS*cm^{-2}	"
gKm	0.1 mS*cm^{-2}	Smith et al., 2013 (17)
gKca	0.3 mS*cm^{-2}	"
gCa	0.05 mS*cm^{-2}	"
gCaT	0.15 mS*cm^{-2}	"

Movie S1. Illustration of dendritic activity on the neural morphology.
The video illustrates synaptic input (circles, color- and size coded by synaptic strength) and dendritic activity (colors on morphology, initiations of dendritic Na^+ spikes, NMDA spikes and bAPs indicated by triangles) from which the maximum voltage projection in Fig. 3*B* has been computed.